Title

Neuronal PAS domain 2 (Npas2) facilitated osseointegration of titanium implant with rough surface through a neuroskeletal mechanism.

Authors

Morinaga, Kenzo
Sasaki, Hodaka
Park, Sil
et al.

Publication Date

2019-02-01

DOI

10.1016/j.biomaterials.2018.11.003

Peer reviewed

Contents lists available at ScienceDirect

Biomaterials

journal homepage: www.elsevier.com

Neuronal PAS domain 2 (*Npas2*) facilitated osseointegration of titanium implant with rough surface through a neuroskeletal mechanism

Kenzo Morinaga[a, b], Hodaka Sasaki[a, c], Sil Park[a], Akishige Hokugo[a, d], Hiroko Okawa[a, e], Yu Tahara[f], Christopher S. Colwell[f], Ichiro Nishimura[a, *]

[a] Weintraub Center for Reconstructive Biotechnology, UCLA School of Dentistry, Los Angeles, CA, USA
[b] Department of Oral Rehabilitation, Section of Oral Implantology, Fukuoka Dental College, Fukuoka, Japan
[c] Department of Oral and Maxillofacial Implantology, Tokyo Dental College, Tokyo, Japan
[d] Regenerative Bioengineering and Repair Laboratory, Division of Plastic and Reconstructive Surgery, Department of Surgery, David Geffen School of Medicine at UCLA, Los Angeles, CA, USA
[e] Division of Molecular and Regenerative Prosthodontics, Tohoku University Graduate School of Dentistry, Sendai, Japan
[f] Department of Psychiatry & Biobehavioral Science, David Geffen School of Medicine at UCLA, Los Angeles, CA, USA

ARTICLE INFO

Keywords:
Titanium biomaterials
Endosseous implant
Osseointegration
Npas2
Chemical genetics
Neuroskeletal regulation

ABSTRACT

Titanium (Ti) biomaterials have been applied to a wide range of implantable medical devices. When placed in bone marrow, Ti-biomaterials integrate to the surrounding bone tissue by mechanisms that are not fully understood. We have previously identified an unexpected upregulation of circadian clock molecule neuronal PAS domain 2 (*Npas2*) in successfully integrated implant with a rough surface. This study aimed to elucidate the molecular mechanism of osseointegration through determining the role of *Npas2*. Human bone marrow stromal cells (BMSC) that were cultured on a Ti disc with SLA surface exhibited increased *NPAS2* expression compared to BMSC cultured on a machined surface. A mouse model was developed in which miniature Ti implants were surgically placed into femur bone marrow. The implant push-out test and bone-to-implant contact measurements demonstrated the establishment of osseointegration in 3 weeks. By contrast, in *Npas2* functional knockout (KO) mice, the implant push-out value measured for SLA surface Ti implant was significantly decreased. *Npas2* KO mice demonstrated normal femur bone structure surrounding the Ti implant; however, the recovered implants revealed abnormal remnant mineralized tissue, which lacked dense collagen architecture typically found on recovered implants from wild type mice. To explore the mechanisms leading to the induced *Npas2* expression, an unbiased chemical genetics analysis was conducted using mouse BMSC carrying an *Npas2*-reporter gene for high throughput screening of Library of Pharmacologically Active Compounds. *Npas2* modulating compounds were found clustered in regulatory networks of the α2-adrenergic receptor and its downstream cAMP/CREB signaling pathway. Mouse primary BMSC exposed to SLA Ti disc significantly increased the expression of α2-adrenergic receptors, but the expression of β2-adrenergic receptor was unaffected. Our data provides the first evidence that peripheral clock gene component *Npas2* plays a role in facilitating the enhanced osseointegration through neuroskeletal regulatory pathways induced by BMSC in contact with rough surface Ti implant.

1. Introduction

Titanium (Ti)-based biomaterials have been widely used in implantable medical devices for orthopedic [1] and dental [2] applications. In a classic study, Laing et al. (1967) examined the tissue reaction of metallic materials implanted in rabbit muscle and concluded that commercially pure Ti and Ti alloys were among those which induced the least foreign body reaction and minimal fibrosis [3]. The osseointegration of Ti-implants was initially explained by the establishment of direct bone to implant connection without a layer of soft tissue encapsulation owing to relatively inert Ti biomaterials [4]. However, surface functionalization of Ti implants has been shown to improve and accelerate the osseointegration process includes moderately rough surface topography [5] and nanotopography [6,7], increasing surface energy [8,9] as well as incorporating bone inductive biological molecules [10]. The outcome of these functionalization technologies suggest that Ti-biomaterials with a complex surface can induce biological reactions

* Corresponding author. Weintraub Center for Reconstructive Biotechnology, UCLA School of Dentistry, Box 951668, CHS B3-087, Los Angeles, CA 90095, USA.
Email address: inishimura@dentistry.ucla.edu (I. Nishimura)

https://doi.org/10.1016/j.biomaterials.2018.11.003
Received 25 July 2018; Received in revised form 1 November 2018; Accepted 2 November 2018
Available online xxx
0142-9612/

leading to the establishment of enhanced osseointegration, although the underlying mechanisms are not yet fully understood.

Several reports from experimental animal studies and human cases suggest that vitamin D levels are a critical factor determining successful osseointegration [11–14]. While it is well established that activated vitamin D in the kidney controls calcium ions in the circulation; its precise action in bone tissue is less understood [15]. The impaired osseointegration in vitamin D deficient rats was not due to failure of bone formation around implant but is rather driven by the decreased bone bonding to the implant surface [16,17]. To determine the role of vitamin D in implant osseointegration, we previously performed a whole genome microarray study of peri-implant tissue derived from vitamin D sufficient and deficient rats. This study unexpectedly identified the molecular circadian clock gene Neuronal PAS domain protein 2 (*Npas2*) as highly associated with the successful development of osseointegration [16].

Npas2 is a transcription factor containing a basic helix-loop-helix (bHLH) structure for DNA binding [18]. Due to a sequence similarity with Circadian Locomoter Output Cycles Kaput (*Clock*), *Npas2* has been considered a member of core circadian rhythm regulatory molecules [19]. Centrally, circadian rhythms are generated by timing system found in the hypothalamic suprachiasmatic nucleus (SCN). On a molecular level, the core clock molecules Brain and Muscle Arnt-like protein 1 (*Bmal1*) and *Clock* dimerize to participate in a transcription/translation feedback loop involving Period (*Per*) and Cryptochrome (*Cry*) molecules [18]. Molecular circadian rhythms are also found in peripheral tissues including bone. Mouse calvarial bone organ culture demonstrated that the bone mineral deposition occurred with a circadian cycle [20]. A microarray analysis of mouse calvaria revealed the presence of peripheral circadian rhythm in bone and demonstrated that the expression of nearly 30% of all genes followed the 24-h cycle [21]. Recently, Ti disc with a complex surface was found to upregulate *Npas2* expression of bone marrow stromal cells (BMSC) *in vitro*, while *Per* gene expression was down regulated. The weighed gene co-expression network analysis revealed that the up-regulation of *Npas2* driven by the Ti implant was selective and not seen in other circadian rhythm-related genes [22], suggesting that an independent molecular mechanism was responsible for the increased *Npas2* expression in response to Ti-biomaterials.

These observations have led to our hypothesis that *Npas2* in peri-implant tissue plays an important role in the establishment of osseointegration. To address this hypothesis, we evaluated implant osseointegration in mice carrying *Npas2* functional knockout (KO) mutation. We report here that enhanced osseointegration of Ti implant with rough surface was significantly attenuated in *Npas2* KO mice. Furthermore, an unbiased chemical genetics screen to elucidate the signaling pathways leading to Ti biomaterials-induced *Npas2* implicated an altered neuroskeletal regulation as a possible mechanism involved in the establishment of enhanced osseointegration.

2. Materials and methods

2.1. Ethics statement

All of the experimental protocols using animals were reviewed and approved by the UCLA Animal Research Committee (ARC# 1997-136) and followed the PHS Policy for the Humane Care and Use of Laboratory Animals and the UCLA Animal Care and Use Training Manual guidelines. All of the animals had free access to food and water and were maintained in regular housing with a 12-12 h light/dark cycle.

2.2. Ti-biomaterial surface modifications

For *in vitro* studies, commercially pure Ti discs (32 mm in diameter and 1 mm thick) were fabricated. The surface of the Ti discs was treated by sandblasting with large grits and acid etched (SLA) using the production protocols for commercially available dental implants (Neobiotech USA, Inc. Los Angeles, CA). Briefly, Ti discs were cleaned and degreased by acetone bath, and then processed in a 2% ammonium fluoride/2% hydrofluoric acid/10% nitric acid solution at 55 °C for 30 s to produce the pretreatment surfaces. SLA surfaces were created by coarse-grit blasting the disks with 0.25–0.50 mm corundum followed by acid etching in a mixture of HCl and H_2SO_4. Control Ti discs were left as machined. The discs were cleaned, gas sterilized and packaged individually.

For *in vivo* studies in mice, rod-shaped experimental Ti implants (4 mm long and 0.6 mm diameter) were designed to fit to mouse femur bone marrow. The surface of Ti implants were treated with SLA or left as machined as above. Each Ti implant connected with a handle and was gas sterilized and packaged individually.

2.3. Surface characterization of Ti discs

SLA and machined surface Ti discs were used for the surface roughness characterization. Surface roughness measurement was performed by photogrammetric technique [23]. Three eucentric tilted (angle 5°) 2D images per each region of interest (ROI) were obtained using scanning electron microscopy (SEM; Nova 230 Nano SEM, FEI, Hillsboro, OR, USA). Three-dimensional (3D) surfaces based on these SEM images were reconstructed and 3D optical interferometric profilometry (n = 3 in each group) was performed with photogrammetry technique software (MeX, Alicona Imaging GmbH, Raaba, Graz, Austria). Eight hundred (800) μm of filter value (cutoff value λc) was applied to detect the contour appropriately.

Hydrophilicity drop test was performed to evaluate the surface wettability of samples. The 1 μl of double-distilled water was dropped and the standardized lateral photographs were obtained at 10 s after application (n = 5 per each sample). The contact angle of drops was measured in the digitized images using a Java-based image-processing program (Image J ver.1.51, NIH, Bethesda, MD).

Behavior and cytoskeletal arrangement of bone marrow stromal cells (BMSCs: iMSC3, Applied Biological Materials, Richmond, BC, Canada) seeded onto polystyrene, Ti disc with machined surface and SLA surface, CoCr disc, zirconia disc were also examined. Twenty-four [24] hrs after seeding, Hoechst 33342 (Thermo Fisher Scientific, Waltham, MA, USA) was applied to visualize the nucleus and then cells were fixed in 10% paraformaldehyde and stained with rhodamine phalloidin (Molecular Probes, Eugene, OR, USA). Stress fibers were observed using fluorescence microscope (DMI6000 B; Leica, Wetzlar, Germany).

2.4. Circadian rhythm gene expression in human BMSCs

Human BMSCs (iMSC3, Applied Biological Materials) were cultured (20,000 cells per cm^2) on polystyrene 35-mm culture dishes, machined Ti discs or SLA Ti discs [22]. Starting from 24 to 48 h after the synchronization with 10 μM forskolin, BMSCs from each group were harvested every 4 h, and total RNA was prepared (n = 4 per time point in each group). Taqman-based reverse transcription polymerase chain reaction (RT-PCR) was performed using commercially available probes for *PER1*, *PER2*, *PER3*, *BMAL1*, *CLOCK* and *NPAS2* (Life Technologies, Grand Island, NY). It must be noted that qRT-PCR requires the accurate normalization of genes of interest to a reference housekeeping gene that is stable and unaffected by the circadian cycle. GAPDH, beta-actin

and 18S rRNA are among the most frequently used housekeeping genes. Nakao et al. (2017) tested the expression stability of 13 different housekeeping genes and reported that 18S rRNA was stable in Liver, white adipose tissue and skeletal muscle (efficiency 91.9%, 93.5% and 94.5%, respectively), while GAPDH was stable in white adipose tissue (97.7%) but less stable in other tissues [24]. We have tested GAPDH and beta-actin in the context of circadian rhythm gene expression of BMSC (data not shown). As such, we used GAPDH as a reference housekeeping gene for this study.

The gene expression amplitude and time factors were evaluated by two-way analysis of variance (ANOVA). When significant p value for interaction between gene expression and time factors was obtained, the effect of biomaterial substrates was examined for the each time point by Tukey test.

Furthermore, the circadian rhythmicity was analyzed by harmonic regression. The harmonic model was determined by:

$Y = \text{intercept} + \text{linear x } h + \text{Amplitude x } \sin(2\pi/24 \times (h - d)) + \text{error}$

Y: gene expression
h: time (hours)
d: offset in hours
Intercept: value of Y when h = 0
Amplitude: the average maximum gene expression when h-d = 6 h and average minimum gene expression when h-d = 18 h after removing the intercept and linear trend.

The detrended harmonic regression plots [25] were generated by the intercept subtracted and the learn trend removed. We used the detrended harmonic regression plots to compare the effect of substrates on circadian rhythmicity by comparing the amplitudes.

Separately, forskolin-synchronized human BMSC was cultured on Ti disc with machined surface, CoCr and Zirconia discs. Cell were harvested at 32 h time point and total RNA samples were prepared. The expression of core circadian rhythm genes was determined as described above.

2.5. Experimental Ti implant placement in mouse femurs

Male 10–15-wk-old C57Bl/6J mice underwent surgical placement of Ti implants following the published orthopedic implant protocol [26] with several refinements. After anesthesia with isoflurane inhalation, the distal femur was accessed via medial parapatellar arthrotomy with lateral displacement of the quadriceps-patellar complex. After locating the femoral intercondylar notch, the femoral intramedullary canal was manually reamed with a 25-gauge needle for entry into the canal and further reamed with a 23-gauge needle. A Ti implant was inserted in a retrograde fashion into each femur of a mouse. The Ti implant was clipped at 4 mm and further inserted 4 mm using a periodontal probe. The quadriceps-patellar complex was reduced to its anatomic position, and the surgical site was closed using Vicryl 5-0 sutures. Carprofen (5.0 mg/kg) (Rimadyl, Zoetis US, Parsippany, NJ) was administered subcutaneously at the time of surgery and every 24 h for 2 days after surgery.

2.6. Implant push-out measurement of osseointegration

Mice were euthanized and femur bones were harvested at the predetermined healing time. Distal epiphyseal cartilage and the medial half of the femur were removed using a dental diamond disc to locate the implant without overheating. The femurs were then embedded vertically in an acrylic resin block so that the mesial, flat end of the implant was exposed. The mechanical withholding strength was measured by pushing the implant out from the femur bone marrow using a custom-made stainless steel pushing rod mounted on a 1000-N load cell (Instron, Canton, MA). The axial load on the implant was applied at a cross-head speed of 1 mm/min, and displacement of the implant and the load were recorded. The displacement load (N) was used as the implant-push out value.

In the initial study, mice were euthanized 1, 2, 3, 4 and 8 wk after machined (n = 4 at each time point) and SLA (n = 4 at for each time point) implant placement and the time course data were obtained. The time course data were evaluated by two-way ANOVA. Furthermore, the implant push-out data of each time point were compared by Tukey test. In the subsequent studies, the femur samples were harvested 3 wk after implant placement and the data were compared by one-way ANOVA with post hoc Holm test.

2.7. Nondecalcified histology of mouse femurs containing Ti implants –

For implant push-out study, the implant was dislodged from femur bone and thus not suitable for histological study. Thus a separate experiment was conducted for histological study, in which femurs were harvested 1, 2, 3 and 4 wk after Ti implant placement (n = 4 at each time point) and fixed in 10% buffered formalin. Femurs were first subjected to microCT scanning (μCT40, Scanco Medical, Wayne, PA) and then processed for nondecalcified longitudinal histological sections (Ratliff Histology Consultant, LLC, Franklin, TN). Using microCT image as a guide, a histological section (30 μm) from each specimen was prepared by a grounding system and stained with Goldner trichrome. The bone-implant contact ratio (BIC) was determined by the bone-implant linear measurement over the entire implant periphery length using ImageJ ver.1.51. The bone contact to implant was defined as the direct association between bone tissue (stained in red) and implant surface without any other interfering tissues (stained in blue). The time course BIC data were evaluated by two-way analysis of variance (ANOVA). The BIC of SLA and machined implants for each time point was compared by Student's *t*-test.

2.8. Energy-dispersive X-ray spectroscopy (EDS) and scanning electron microscopy (SEM)

After the implant push-out test, the dislocated Ti implants were recovered from femur bones. The implant surface was scanned by EDS (Supra 40VP SEM, ZEISS, Thornwood, NY). EDS analysis was completed in 5 segments, covering the entire length of the implant. The elemental composition of Ti, calcium (Ca) and phosphorous (P) was determined from the mean of the 5 segment measurements for each implant. The recovered implants were further spatter-coated with iridium (Ir) and examined by SEM (Supra 40VP SEM, ZEISS, Thornwood, NY).

2.9. Characterization of femur bone of Npas2 ± and Npas2−/− mice

Npas2 ± mice [27] on the C57Bl/6J background were generated from cryopreserved sperm samples (B6.129S6-Npas2tm1Slm/J, Jackson Laboratory, Bar Harbor, ME), and an active breeding colony was established at UCLA. Genotype was determined by PCR of genomic DNA isolated from ear punch tissues from each mouse. In *Npas2* allele, the basic helix-loop-helix (b-HLH) DNA binding sequence is encoded largely by Exon2, which was replaced by a LacZ reporter gene cassette. The mutant Npas2 protein without bHLH sequence lacked the critical DNA binding activity and thus this mouse model was considered functional knockout (KO) of *Npas2* [27]. The common PCR primer was synthesized to target the intron between Exon1 and Exon2, as well as the WT primer targeting Exon2 and the mutant primer targeting the LacZ reporter gene cassette. PCR reaction with the common and Exon2 primers or LacZ reporter gene primer generated 257 bp or 350 bp PCR

product, respectively. A conventional 2% agarose gel was used to determine the mouse genotype.

The effect of *Npas2* KO mutation was evaluated in femur bone. Femurs from C57Bl6J wild-type (WT: *Npas2*+/+), *Npas2* ± and *Npas2*−/− mice were measured for anatomical length and characterized by micro-CT (μCT-40; Scanco Medical, Brüttiselen, Switzerland). The obtained micro-CT data were analyzed with the proprietary analysis software. For each femur, the volume of interest (VOI) was determined between 996 μm and 2676 μm below the growth plate. After cortical bone was digitally eliminated, the cortical bone was used to determine bone volume/total volume (BV/TV), the number of trabecular bone (Tb.N), the thickness of travecular bone (Tb.Th) and the space between trabecular bones (Tb.Sp). The data of each parameter were compared by Tukey test.

Femurs were also evaluated by EDS for Ca and P elements.

2.10. Implant osseointegration in WT, Npas2 ± and Npas2−/− mice

Male 10–15-wk-old WT (n = 12 for each implant group), *Npas2*+/− (n = 8 for each implant group) and *Npas2*−/− (n = 4 for each implant group) mice received SLA or machined Ti implants in their femurs, as described. Three [3] weeks after the implant placement, mouse femurs were harvested, and the implant push-out test was conducted. After the implant push-out test, the dislodged Ti implants were carefully recovered from the femur bone marrow and subjected to EDS and SEM analyses. In a separate experiment, 3 weeks after the implant placement, femurs were harvested and processed for non-decalcified longitudinal sectioning of the plastic-embedded femur and implant for histological observation.

2.11. Chemical genetics analysis

Femur BMSC harvested from *Npas2*−/− mice were previously characterized for LacZ expression [22], which was used in this study for high throughput, unbiased screening of Library of Pharmacologically Active Compounds (LOPAC^{1280}). Using 384-well plates, each well was filled with 25 μl non-phenol red DMEM containing 10% FBS and 1% PS, and added 50 nL of LOPAC compound (final concentration: 1 μM) using 500 nL pin tool (Biomek FX, Beckman Coulter, Indianapolis, IN). To each well, BMSC (*Npas2*-LacZ) were placed as 1500 cells/25 μl suspension and incubated at room temperature for 1 h, followed by incubation at 37 °C and 5% CO_2 for 48 h. To measure *Npas2*-LacZ expression, β-galactosidase activity was measured using a commercially available assay (Beta-Glo Assay System, Promega, Summerville, CA).

The *Npas2*-LacZ expression data were uploaded on an online data analysis tool (CDD Vault, Collaborative Drug Discovery, Inc, Burlingame, CA), on which data were normalized and Z-factor was calculated. For this study, hit compounds were selected as Z-score > 2.5 or < -2.5. The selected hit compounds (final concentration: 1 μM) were validated by 3 replicated 384-well plates with mouse BMSC (*Npas2*-LacZ). The compounds significantly increased or decreased the β-galactosidase activity of BMSC as compared to the untreated cells were selected as candidates. The class, mechanism of action and related functions of the candidate compounds were obtained from the CCD Vault database and literature reviews.

2.12. Expression of adrenergic receptors by mouse BMSC

Total RNA isolated from mouse primary BMSC cultured on polystyrene plate, SLA Ti disc or machined Ti disc as described above was examined for the steady state mRNA levels of α1a, α1b, α1d, α2a, α2b, α2c, β1, β2 and β3 adrenergic receptors using Taqman-based RTPCR. The data were compared by Tukey test.

3. Results

3.1. Human BMSCs exposed to Ti biomaterials modulated the circadian expression pattern of clock genes

This study used machined and SLA-treated Ti biomaterials. The surface micro-topographic characteristics (Fig. 1A–C) were consistent with published data [28]. The contact angles of polystyrene culture plate, machined and SLA Ti discs were within a similar range (Fig. 1D) and consistent with the published data [29]. We also characterized the Ti disc by examining BMSC behaviors. It has been well established that the development of F-actin stress fibers and cell shapes were influenced by the substrate micro-structures [30] and surface energy [31]. The fluorescent F-acting staining revealed the cells widely spread on polystyrene plates. By contrast, cell shapes were affected by the surface isotropic and anisotropic topography of machined and SLA discs, respectively (Fig. 1E).

Since the clock genes oscillate with a 24-hr cycle length, we tested the effect of Ti discs on the clock gene expression in every 4 h for 24 h in synchronized cells. Forskolin-synchronized human BMSCs maintained on a conventional culture plate demonstrated a circadian expression of *PER1, PER2,* and *PER3* with a peak expression between 36 and 44 h (Fig. 2A), which was consistent with our previous observation [22]. Two-way ANOVA resulted the statistically significant p values of interaction between the culture substrate materials and time in *NPAS2* and *PER2*. The effect of culture substrate materials evaluated by Tukey test for each time point revealed that when BMSCs were exposed to the SLA disc, there was a striking upregulation of *NPAS2* throughout the 24-hr period (Fig. 2B).

The *NPAS2* and *PER2* expression data were further analyzed by the harmonious regression analysis and the detrended harmonious regression analysis (Fig. 2C). These analysis tools were used to evaluate if *NPAS2* and *PER2* expression followed a circadian rhythm in this cell population. The error is the difference between Y and the value predicted by the harmonic regression model. The error (as measured by the standard division) is small if the model is a good fit to the data while an R square value is less than 0.50 (50%) implies a poor model fit to the data. Based on our statistical analyses, SLA drives the loss of circadian rhythmicity of *NPAS2* and *PER2* (Fig. 2D). The detrended harmonic regression plots of *NPAS2* and *PER2* were generated by the intercept subtracted and the learn trend removed. We used the detrended harmonic regression plots to compare the effect of substrates on circadian rhythmicity by comparing the amplitudes (Fig. 2D). Again, we found that SLA decreased the circadian expression of both *NPAS2* and *PER2* in these cells. The machined Ti disc generated a similar reduction in clock gene expression although the effect was less significant.

In an additional experiment, we examined clock gene expression in cells grown on zirconia and CoCr discs, whose surfaces were not modified. The result showed that the pattern of clock gene expression of zirconia disc was highly consistent with machined Ti disc, whereas CoCr disc showed a different clock gene expression pattern; however, *NPAS2* upregulation was not clearly observed in either zirconia or CoCr discs (Fig. S1).

3.2. Ti implant placed in mouse femur demonstrated osseointegration

Prior work has examined the impact of Ti implant in mouse bone by placing a Ti wire retrograde into the bone marrow space of femurs through epiphyseal cartilage and growth plate [32,33], or a small rod or screw was perpendicularly inserted in the middle of femurs [34–37]. In the present study, an experimental Ti implant with machined or SLA surface was placed in the distal half of the mouse femur bone marrow

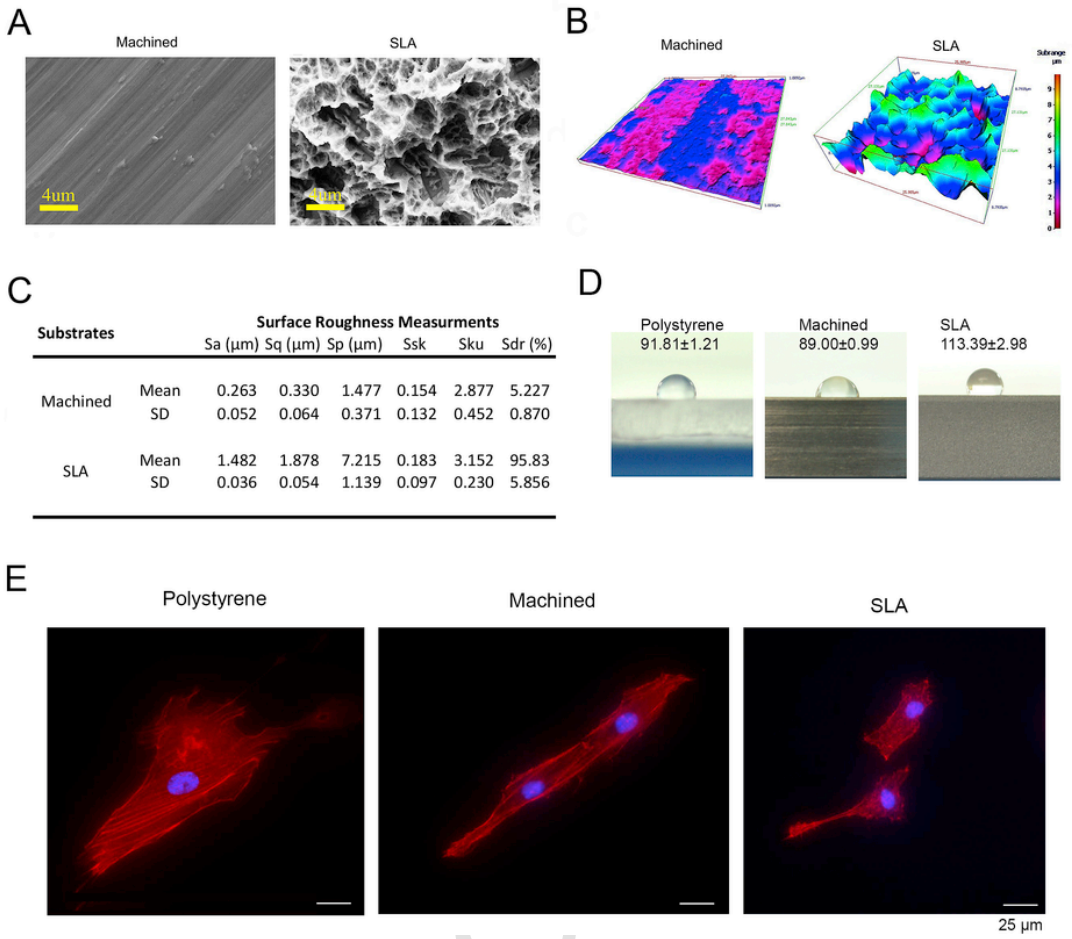

Substrates		Surface Roughness Measurments					
		Sa (μm)	Sq (μm)	Sp (μm)	Ssk	Sku	Sdr (%)
Machined	Mean	0.263	0.330	1.477	0.154	2.877	5.227
	SD	0.052	0.064	0.371	0.132	0.452	0.870
SLA	Mean	1.482	1.878	7.215	0.183	3.152	95.83
	SD	0.036	0.054	1.139	0.097	0.230	5.856

Fig. 1. Surface and biological characterization of Ti discs. **A**. SEM images of commercially pure Ti discs treated as machined or sand blasted and acid etched (SLA) demonstrated isotropic and anisotropic surface topography, respectively. **B**. Three-dimensional (3D) surfaces of machined and SLA Ti discs were reconstructed from SEM images. **C**. Surface roughness measurements by 3D optical interferometric profilometry (n = 3 in each group) were performed with photogrammetry technique software. **D**. Hydrophilicity drop test for polystyrene culture plate, machined and SLA Ti discs demonstrated the relatively hydrophobic nature of these substrates. **E**. Human BMSC cultured on polystyrene culture plate, machined and SLA discs demonstrated the development of F-actin stress fibers (red) following the surface topography of substrates. Nucleus was stained by Hoechst 33342 (blue). (For interpretation of the references to colour in this figure legend, the reader is referred to the Web version of this article.)

without contact with epiphyseal cartilage and growth plate (Fig. 3A–C). The mechanical withholding shear strength is a hallmark of successful osseointegration. The implant push-out test was designed to measure load at the shear break point in this study (Fig. 3D). The implant push-out test demonstrated the development of mechanical withholding strength in both SLA and machined implants, while the former generated much higher implant push-out values than the latter. The push-out value of the SLA implant increased 3 wks after implant placement and reached a plateau with a noticeable transient decrease at 4 wks (Fig. 3D). The BIC ratio of the SLA implant measured in nondecalcified histological sections revealed a progressive increase from 1 to 3 wks, followed by a plateau (Fig. 3F). By contrast, there was a slow increase in the BIC ratio of the machined implant. It must be noted that BIC ratios, particularly of machined implant showed significant variations (Fig. 3F). While the identification of bone-implant contact of SLA implants was clearly observed, the histological determination of bone-machined implant contact required a careful interpretation.

The dislodged Ti implant after the push-out test was subjected to SEM/EDS analysis (Fig. 3H). The implant surface elements were largely Ti, Ca, P and O (Fig. 3I). The weight % of Ti of the recovered SLA implants progressively decreased from 1 to 3 wks and reached a plateau, whereas that of the recovered machined implants remained 90% throughout the healing period (Fig. 3J).

3.3. The lack of femur bone abnormalities in *Npas2* ± and *Npas2*−/− mice

The functional bHLH domain of *Npas2* is largely encoded by exon 3, which was replaced by a LacZ/Neo cassette (Fig. 4A), resulting in the synthesis of Npas2 molecules without DNA binding bHLH domains [27]. Femurs harvested from WT, *Npas2* ± and *Npas2*−/− mice were indistinguishable in terms of anatomical size and shape (Fig. 4B) and the interior trabecular bone architecture depicted by 3D reconstructed microCT images (Fig. 4C). The quantitative 3D bone morphometric analyses showed that *Npas2* KO mice exhibited comparative data of bone volume/total volume (BV/TV), the number of trabecular bone (Tb.N), the thickness of trabecular bone (Tb.Th) and the space between trabecular bones (Tb.Sp) (Fig. 4D). *Npas2* KO mutation did not affect bone architecture or remodeling and thus *Npas2* KO mice were determined to be a suitable mouse model for investigating the mechanism of implant osseointegration in this study.

3.4. *Npas2* KO mutation decreased implant osseointegration with the SLA surface but not with the machined surface

We examined the role of *Npas2* on osseointegration after 3 wks of implant placement in femurs of *Npas2* KO mice. The push-out value of

A

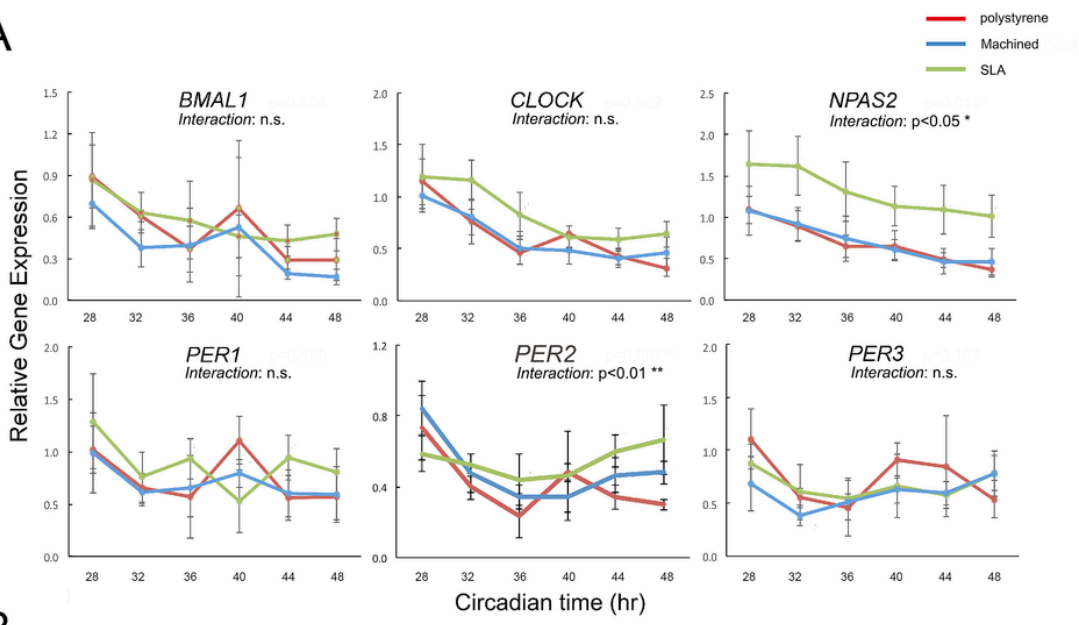

B

gene	substrates	28 hr	32 hr	36 Hr	40 hr	44 hr	48 hr
NPAS2	Polystyrene vs. Machined	n.s.	n.s.	n.s.	n.s.	n.s.	n.s.
	Polystyrene vs. SLA	p<0.05*	**p<0.01****	**p<0.01****	**p<0.01****	**p<0.01****	**p<0.01****
	Machined vs. SLA	p<0.05*	**p<0.01****	**p<0.01****	**p<0.01****	**p<0.01****	**p<0.01****
PER2	Polystyrene vs. Machined	n.s.	n.s.	n.s.	n.s.	n.s.	p<0.05*
	Polystyrene vs. SLA	n.s.	n.s.	p<0.05*	n.s.	**p<0.01****	**p<0.01****
	Machined vs. SLA	p<0.05*	n.s.	n.s.	n.s.	p<0.05*	p<0.05*

C

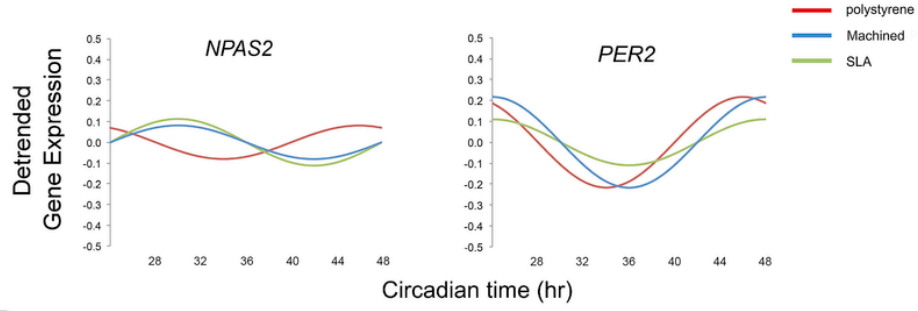

D

gene	substrate	offset=d	intercept	linear	Amplitude	Amplitude SE	R square	error SD	amplitude comparisons across substrates	
NPAS2	Polystyrene	4	1.26	-0.041	-0.081	0.0051	75.0%	0.1443	Polystyrene vs. Machined	**p<0.01****
	Machined	0	1.08	-0.027	0.081	0.0071	57.8%	0.2022	Polystyrene vs. SLA	**p<0.01****
	SLA	0	1.68	-0.027	0.112	0.0109	**40.9%**	**0.3104**	Machined vs. SLA	p<0.05*
PER2	Polystyrene	4	0.85	-0.031	-0.217	0.0042	62.9%	0.1191	Polystyrene vs. Machined	p=0.936
	Machined	6	0.81	-0.023	-0.217	0.0026	75.7%	0.0985	Polystyrene vs. SLA	**p<0.01****
	SLA	6	0.55	0.000	-0.110	0.0040	**22.6%**	**0.1496**	Machined vs. SLA	**p<0.01****

Fig. 2. SLA Ti disc significantly affected the circadian expression of *NPAS2* and *PER2* of human BMSC. **A.** Time course expression of clock genes by human BMSC cultured on polystyrene culture plates, machined Ti discs and SLA Ti discs (n = 6 per time point in each group). The data were evaluated by two-way ANOVA. The statistical significance of interaction between substrates and time was achieved in *NPAS2* and *PER2*. *: $p < 0.05$; **: $p < 0.01$. **B.** The expression data of *NPAS2* and *PER2* were further evaluated by Tukey test for each time point. *NPAS2* expression was significantly increased when BMSCs were cultured on SLA Ti discs. **C.** Detrended harmonious regression analysis of *NPAS2* and *PER2* expression. **D.** Statistical evaluation of the harmonious regression and detrended harmonious regression analyses. The harmonious regression model of circadian rhythm was compared to the raw data. R square <50% and large error (SD) suggested that SLA Ti disc disrupts circadian rhythms in *NPAS2* and *PER2* expression. The detrended harmonious regression analysis suggested SLA Ti disc significantly affected *NPAS2* and *PER2* expression.

the SLA implant was significantly decreased in both *Npas2* ± and *Npas2*−/− mice as compared to WT mice (Fig. 5A). However, the push-out value of the machined implant was not affected by *Npas2 KO* mutation. Nondecalcified histology revealed the formation of bone tissue around Ti implants in WT and *Npas2* KO mice. The bone and implant contact appeared to occur in WT and *Npas2* KO mice (Fig. 4B). The ex-

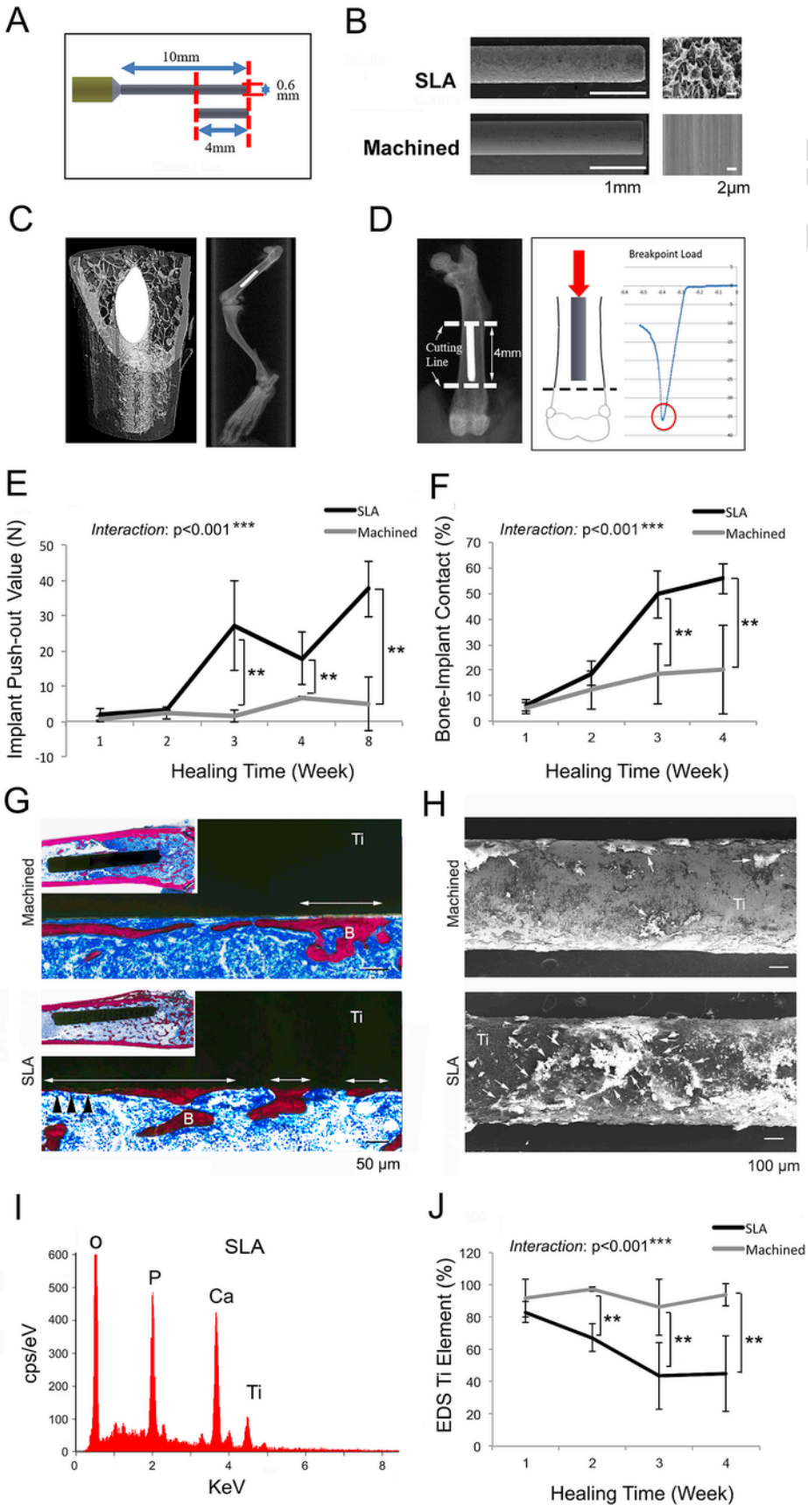
A
10mm
0.6 mm
4mm
B
SLA
Machined
1mm
2μm
C
D
Cutting Line
4mm
Breakpoint Load
E
Interaction: p<0.001***
SLA
Machined
Implant Push-out Value (N)
Healing Time (Week)
F
Interaction: p<0.001***
SLA
Machined
Bone-Implant Contact (%)
Healing Time (Week)
G
Machined
SLA
Ti
B
50 μm
H
Machined
SLA
Ti
100 μm
I
SLA
O
P
Ca
Ti
cps/eV
KeV
J
Interaction: p<0.001***
SLA
Machined
EDS Ti Element (%)
Healing Time (Week)

Fig. 3. Development of mouse implant osseointegration model. **A.** Experimental implants (0.6 mm in diameter and 10 mm in length) were designed with a handle. After insertion into an osteotomy site created in the femur bone marrow, the Ti rod was clipped to generate a 4-mm-long implant. **B**. The surface of the experimental implant was treated as machined or SLA. **C**. A 4-mm implant was placed in the femur bone marrow at a depth of 4 mm from the distal femur joint surface to avoid contact with the epiphyseal cartilage and growth plate. **D**. At predetermined times, mouse femurs were harvested and trimmed to expose the edge of the implant. The mechanical withholding strength of the implant was measured by the implant push-out test. The breakpoint load (N) was determined as the implant push-out value. **E**. The implant push-out value increased over the healing time until 3 wks and then reached a plateau. Two-way ANOVA determined the statistical significance for interaction between the implant types and time. The implant push-out values of SLA and Machined implants were compared by Student's t-test for each time point (n = 4 at each time point) **: $p < 0.01$. **F**. In a separate experiment, bone-to-implant contact ratio was determined. Two-way ANOVA suggested the statistical significance in interaction between implant types and time. The BIC for each time point was compared by Student's t-test for each time point (n = 5 for each group). **: $p < 0.01$. A large variation was noted in the Machined implant group. **G**. For BIC analysis, the harvested mouse femurs were fixed in 10% buffered formalin and processed for nondecalcified epoxy resin-embedded histological sections and Goldner trichrome-staining. There was a trend that trabecular bone around implant was formed at the epiphyseal side than the center of the femur. The bone (red)-to-implant contact (double-head arrows) was defined without interfering bone marrow tissue (blue). The histological appearance of bone-to-implant contact was different between Machined and SLA implants. **H**. After push-out test, implants were recovered from femurs and subjected to SEM/EDS evaluation. Machined implant showed largely exposed Ti implant surface (Ti) with limited remnant tissue coverage (arrows). SLA implant was extensively covered by remnant tissues (arrows) with some Ti surface exposure. **I**. A representative EDS elemental analysis of a 3-wk implant recovered after the push-out test. The remnant tissue contained O, P and Ca elements, whereas the Ti element was decreased. **J**. The entire surface of recovered implant was analyzed by EDS, and the average elemental weight % of Ti was calculated for each implant. The Ti weight % of SLA implants progressively decreased over the healing time until 3 wks and then reached a plateau, whereas that of Machined implants did not decrease. Ti elemental analysis by EDS mirrored the reverse trend of the BIC of SLA implant but not of Machined implant. Two-way ANOVA indicated the statistical significance between the implant types and time. The Ti weight % at each time point was compared by Student's t-test (n = 4 for each time point and each group). **: $p < 0.01$. (For interpretation of the references to colour in this figure legend, the reader is referred to the Web version of this article.)

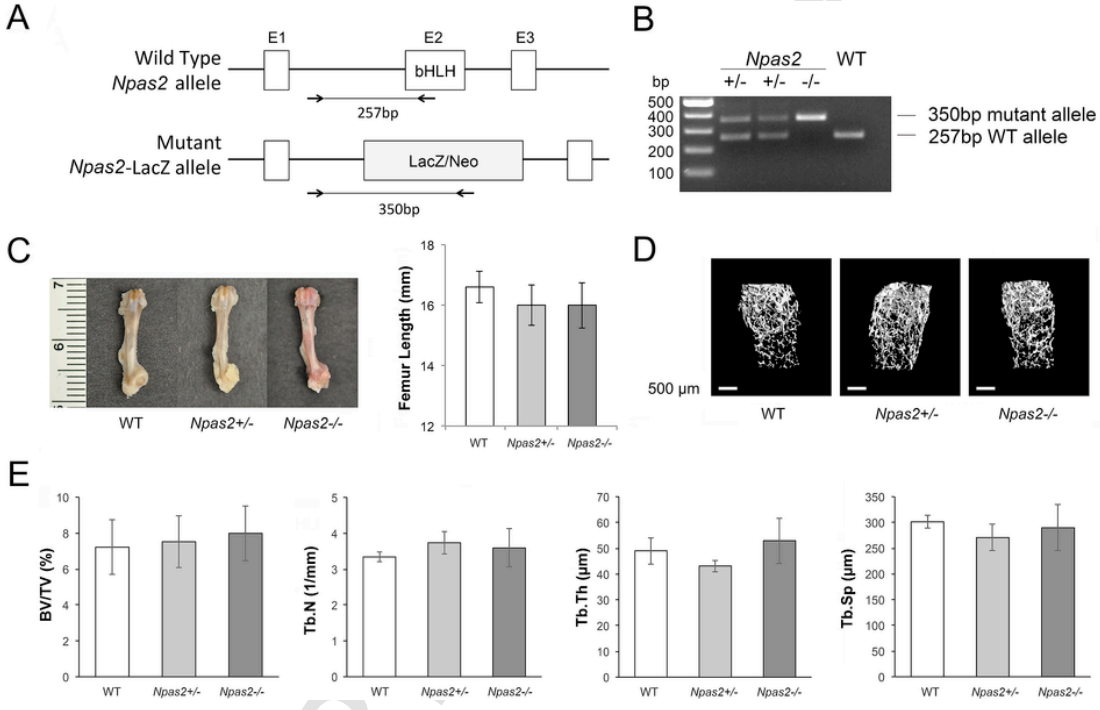

Fig. 4. Femur bone characterization of wild type (WT), *Npas2* ± and *Npas2*−/− mice. **A.** Diagram of *Npas2* allele. Exon2 (E2) encodes the DNA binding basic helix-loop-helix (bHLH) sequence of Npas2, which was replaced with a LacZ expression reporter cassette (LacZ/Neo), as the result, the mutant Npas2 protein lacked the DNA binding function. Genotyping PCR was designed to depict WT *Npas2* allele with the common forward primer in the intron between E1 and E3 and the reverse primer in E2, which gave rise to a PCR product of 275 bp. The mutant allele was detected by the common forward primer and the reverse primer in the LacZ/Neo sequence, which resulted in a 350 bp PCR product. B. An agarose gel electrophoreses revealed the presence of 257 bp PCR product (WT genotype) and 350 bp PCR product (*Npas2*−/− genotype). *Npas2* ± genotype was determined by the both PCR products. **C.** The size and shape of femurs (n = 3 per group) from 15-wk-old WT, *Npas2* ± and *Npas2*−/− mice were indistinguishable. **D.** Micro-CT three-dimensional trabecular bone structure of femurs. **E.** Quantitative analysis of femur trabecular bone structure (n = 6 per group) was evaluated by micro-CT for bone volume/total volume (BV/TV), the number and the thickness of trabecular bone (Tb.N and Tb.Th, respectively) as well as the space between the trabecular bones (Tb.Sp). No significant differences were observed.

perimental implants were recovered after the push-out test and subjected to SEM/EDS analysis. The surfaces of the SLA implants recovered from WT mice were widely covered by tissue remnants, whereas those recovered from *Npas2* ± and *Npas2*−/− mice had tissue remnants of a unique reticular structure with numerous punch holes exposing the Ti substrate, whereas the machined implants were free from tissue attachment (data not shown).

The EDS analysis revealed the much higher Ti content in implants recovered from *Npas2* ± and *Npas2*−/− mice than in those recovered from WT mice (Fig. 5C), indicating that there was small but distinct loss of tissue interaction to SLA Ti implant in *Npas2* KO mice. However *Npas2* KO mutation did not affect the Ca/P ratio of the remnant tissue on the recovered implant as well as femur cortical bone (Fig. 5D).

3.5. Abnormal tissue formed on SLA implant placed in Naps2 ± and Npas2−/− mice

We then examined if the interface tissue coverage affected the implant mechanical withholding strength. The coverage area by the interface tissue was estimated from the Ti weight % on the entire surface of implant: $2\pi 0.6 \times 4.0 \times (100\text{-Ti\%})/100$ (mm^2). A regression analysis revealed a positive correlation between the estimated tissue coverage area and implant push-out value in WT mice ($R^2 = 0.551$, Fig. 5E). By contrast, there was no correlation between the tissue coverage area and the implant push-out value of implants placed in *Npas2 KO* mice. These data indicate that *Npas2 KO* mutation affected the interface tissue facilitating the bone and implant bonding. High-magnification SEM images

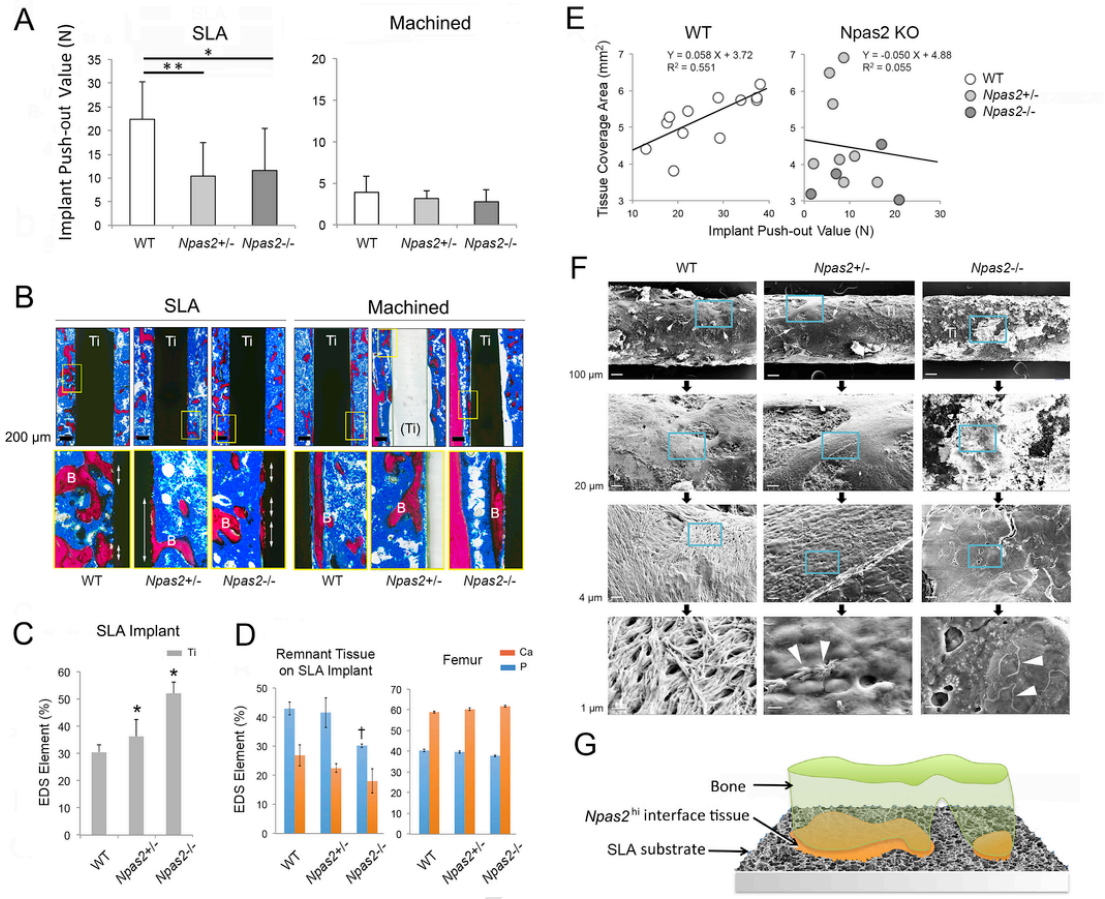

Fig. 5. Impaired osseointegration in *Npas2* ± and *Npas2*−/− mice. **A**. After 3 wks of implant placement, the implant push-out values of SLA implants placed in *Npas2*+/− (n = 8) and *Npas2*−/− (n = 4) mice were significantly smaller than that of WT mice (n = 12). The implant push-out value of machined implants in WT (n = 12), *Npas2*+/− (n = 8) and *Npas2*−/− (n = 4) mice did not show a significant difference. **B**. Nondecalcified histological sections showed bone formation (red: B) around the implant (Ti), which appeared to be unaffected by *Npas2* ± and *Npas2*−/− mutation. The bone-to-implant contact (double-head arrows) was also observed on SLA implants in all genotypes. However, the bone-to-implant contact on the machined implant was not clearly observed. Due to variations among sections, quantitative measurements were not performed. Note: (Ti) indicates the space of implant, which was removed during the histological section preparation; however, bone and bone marrow tissues were well preserved. **C**. EDS elemental analysis revealed larger Ti exposure of SLA implants recovered from *Npas2*+/− (n = 8) and *Npas2*−/− (n = 4) mice than in those recovered from WT mice (n = 12). *: $p < 0.05$ against WT control. **D**. EDS analysis of Ca and P of the remnant tissue on SLA implants and the femur cortical bone of WT, *Npas2* ± and *Npas2*−/− mice. **E**. The tissue coverage area on SLA implant was estimated from the Ti elemental analysis and correlated with the implant push-out value. In WT mice, the estimated tissue coverage area and the implant push-out value was positively correlated, whereas these values did not correlate in *Npas2* ± and *Npas2*−/− mice. **F**. SEM evaluation of SLA implant recovered from WT, *Npas2* ± and *Npas2*−/− mice after push-out test. The remnant tissue coverage (arrows) and implant exposure (Ti) were clearly observed. The high magnification observations revealed dense collagen fibers in the remnant tissue of SLA implants recovered from WT mice, whereas collagen fiber structures were not observed in the remnant tissues of *Npas2* ± and *Npas2*−/− mice. The surface of the remnant tissue of *Npas2* KO mice was relatively smooth with occasional extracellular matrix-like molecules (arrowheads). **G**. A proposed diagram of *Npas2*^{hi} interface tissue generated by the presence of Ti substrate with rough surface, which connects to bone in order to achieve osseointegration. (For interpretation of the references to colour in this figure legend, the reader is referred to the Web version of this article.)

depicted well-developed collagen fibers with a crisscrossed structure in the remnant tissue on the implant recovered from WT mice (Fig. 5F). The collagen structure was less visible in tissue remnants on the implants recovered from *Npas2* ± and *Npas2*−/− mice. Contact guidance refers to the phenomenon that cells adjust their orientation and shape according to the patterns of the substrate biomaterials [38]. The effect of contact guidance further extends the signal transduction of adherent cells [39], leading to differential cell behaviors between the rough and smooth surfaces. This study proposes the presence of interface tissue to SLA implant with highly upregulated *Npas2* expression: *Npas2*^{hi} interface tissue (Fig. 5G).

3.6. Chemical genetics analysis suggested that the Npas2 upregulation mechanism involving altered neuroskeletal pathway

Femur BMSC derived from *Npas2*−/− mouse was previously characterized for the expression of LacZ [22], which was used for high throughput screening of LOPAC^{1280} (Fig. 6A). The output screening data were analyzed for the Z score, whose significant cut line as >2.5 or < -2.5 resulted in a total of 24 hits: 7 *Npas2*-upregulation and 16 *Npas2*-downregulation compounds (Fig. 6B). The validation study identified a total of 14 compounds (Fig. 6C), which were subjected to the chemical genetics analysis. *Npas2* upregulating compounds were found to decrease intracellular cAMP or stimulate the α2 adrenergic receptor. By contrast, *Npas2* down regulating compounds stimulate or accumulate cAMP, or induce cAMP response element binding (CREB) activation (Table 1).

The effect of sympathetic nervous system on bone remodeling has been extensively investigated as neuroskeletal regulation [40,41], in which β2-adrenergic receptor of osteoblasts is thought to play a predominant role (Fig. 6D). The unbiased, chemical genetics analysis suggested that the upregulation of *Npas2* could involve the α2-adrenergic receptor. Mouse femur BMSC exposed to Ti discs were examined and found to show a robust increase in the expression of α2A-, α2B- and α2C-adrenergic receptors by SLA disc, while β2-adrenergic receptor was not affected (Fig. 6E).

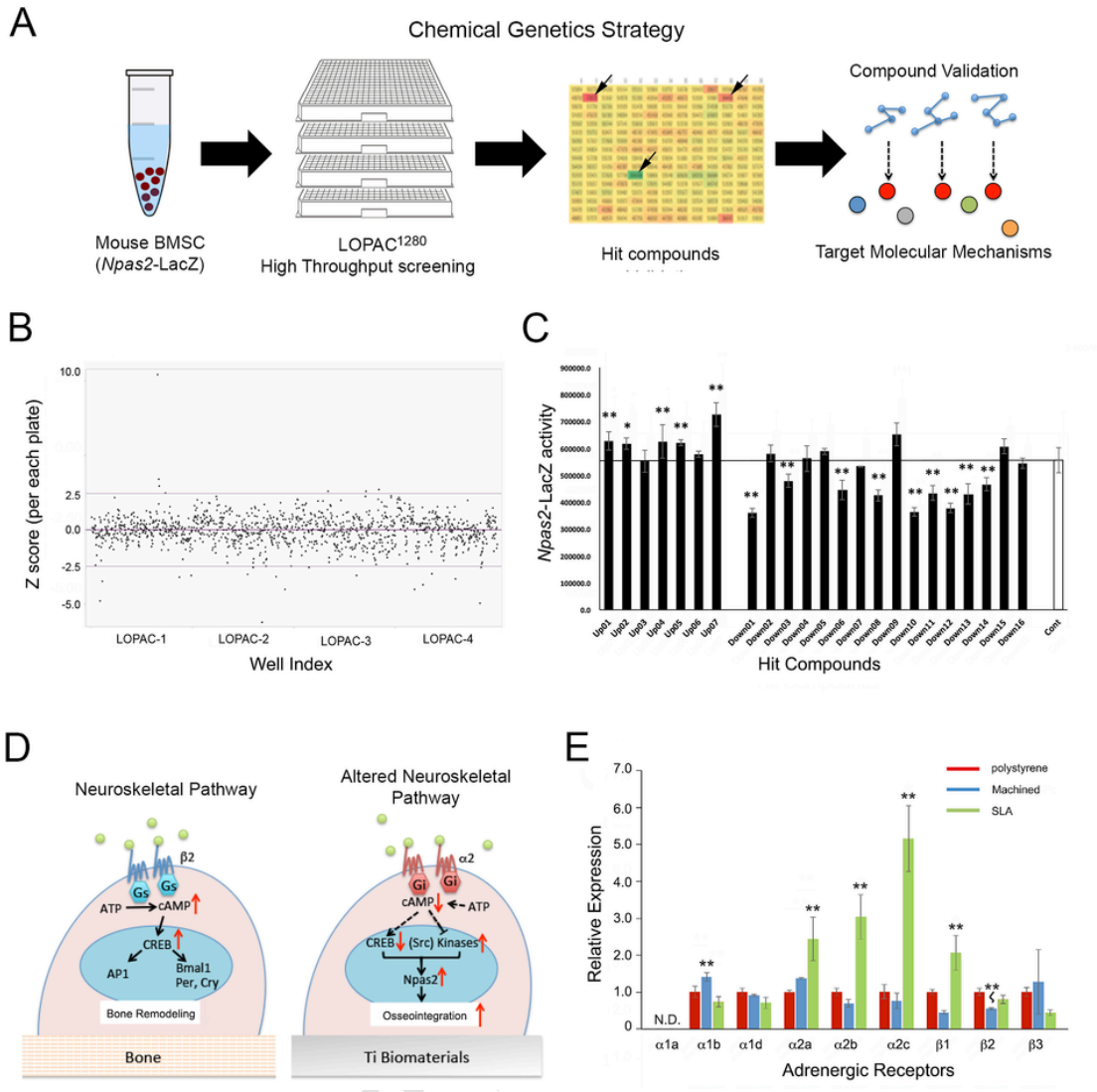

Fig. 6. An unbiased chemical genetics analysis was used to determine the molecular mechanisms underlying implant osseointegration. **A.** A flow diagram of chemical genetics analysis using BMSC carrying *Npas2*-LacZ reporter system. **B.** High throughput screening of LOPAC^{1280} compounds for *Npas2*-LacZ expression of mouse BMSC. Hit compounds were identified as z-score > 2.5 or < -2.5. **C.** Validation of *Npas2*-LacZ expression of hit compounds in triplicated experiments. The compounds (black bars) significantly modulated the *Npas2*-LacZ expression ($p < 0.05$) compared to the untreated control (white bar) were identified. **D.** Neurotransmitter-induced β2-adrenergic receptor in BMSC has been shown to regulate bone remodeling and is referred to as neuroskeletal regulation. The pharmacological actions of identified compounds clustered in the down regulation of cAMP and α2-adrenergic receptors. Altered neuroskeletal regulation was proposed as a molecular mechanism of osseointegration. **E.** Mouse femur BMSC exposed to Ti discs (machined and SLA) were analyzed for the expression of adrenergic receptors. Compared to the conventional culture condition on polystyrene plate, BMSC exposed to SLA Ti disc exhibited significantly upregulated expression of α2-and β1-adrenergic receptors; but not of β2-adrenergic receptor. Turkey test was used to assess statistical significance, which, in this figure, was shown only against the polystyrene control. *: $p < 0.05$; **: $p < 0.01$.

4. Discussion

The results of this study demonstrated the role of *Npas2* in the molecular regulatory mechanisms influencing the successful osseointegration between a Ti implant with a rough surface. Human BMSC exposed to a Ti disc after SLA treatment demonstrated the significant upregulation of *NPAS2* (Fig. 2). This finding was very similar to previous data obtained with Ti disc with Nanotite ™ treatment [22], whereas the effect of the Ti disc on other clock genes appeared to be less consistent. It has been reported that *Npas2* was not detected in mouse femur BMSC and thus could not be involved in bone remodeling and homeostasis [41] (Fig. 3). Our finding suggests that Ti biomaterial-induced *Npas2* regulate BMSC to facilitate successful implant osseointegration.

The present study used a refined mouse femur Ti implant model, which was designed after a previously published mouse orthopedic implant protocol [26]. The osseointegration in SLA implant was established 3 wks after the implant placement by determined by the implant push-out test (Fig. 3E) and BIC data (Fig. 3F). BIC is a widely accepted measurement for the degree of osseointegration and is defined by the histological direct structural and functional connection between living bone and the surface of a load-bearing artificial implant [42]. BIC measurement involves the nondecalcified resin-embedded section through the metallic implant body and histological identification of bone contact to the implant surface. For mouse implant models, the reported BIC of SLA implant was approximately 60–70% for the model with a short implant placed perpendicularly to distal femurs [43], whereas BIC of HA coated implant placed in a longitudinal direction in the femur bone marrow reached approximately 30% [44]. We found that bone-implant contact was more frequently established near the growth plate where more trabecular bone structure was present than the center of femur. Thus, BIC of approximately 50% obtained from SLA implant

Table 1
Chemical Genetics Analysis using Validated Compounds Modulating *Npas2* Expression.

Compounds	Class	Action	Description and Relevant Functions	% Activity[a]
***Npas2* upregulation**				
Up01	Adenosine	Antagonist	Adenosine receptor antagonist with selectivity for A1 over A2 Block β adrenergic receptor-triggered cAMP signaling	104.0
Up02	K + Channel	Inhibitor	Potent Kv1.3 potassium channel inhibitor Kv channel blockers inhibit cAMP-stimulated neuritogenesis	35.3
Up04	Cyclic Nucleotides	Inhibitor	Cyclic nucleotide phosphodiesterase catalyzes the hydrolysis of cAMP and cGMP	26.2
UP05	Serotonin	Antagonist	Semisynthetic ergot alkaloid. Competitive α1 adrenergic receptor blocker and partial α2 adrenergic receptor agonist	28.6
Up07	Biochemistry	Agonist	L-aromatic amino acid decarboxylace inhibitor α-2 adrenergic receptor agonist Decrease intracellular cAMP	18.1
***Npas2* down regulation**				
Down01	Cytoskeleton/ECM	Inhibitor	Fungal metabolite that disrupts the structure and function of the Golgi apparatus	−45.4
Down03	Cytoskeleton/ECM	Inhibitor	Prevents tubulin polymerization Potentiate PGE1 stimulation of cAMP formation	−29.7
Down06	Hormone	Agonist	Potent, cell permeable, subtype selective retinoic acid receptor (RARα) agonist	−25.1
Down08	Nitric Oxide	Inhibitor	Endothelial nitric oxide synthase inhibitor Inhibit cell Redox metabolism; Accumulate cAMP	−18.6
Down10	Cytoskeleton/ECM	Inhibitor	Antineoplastic glycoside; inhibitor of microtubule assembly Induce CREB activation	−15.6
Down11	Cytoskeleton/ECM	Inhibitor	Disrupts microtubules by binding to beta-tubulin	−12.5
Down12	Intracellular Ca++	Releaser	Potent, cell permeable, IP3-independent intracellular Ca++ releaser; Increase intracellular cAMP	−43.5
Down13	Kinase/Phosphatase	Inhibitor	Broad spectrum protein tyrosine kinase inhibitor Inhibit Src and FGFR kinases	−35.5
Down14	Kinase	Inhibitor	Inhibit Src family kinases	−33.0

[a] Activity against negative controls in LOPAC screening.

placed in a longitudinal direction in the femur bone was considered consistent with previous studies. However, the osseointegration for machined implants was not clearly determined by BIC. In histological sections, machined implants showed ambiguous bone association patterns that bone tissue and implant surface showed a gap without a definitive bone marrow tissue (Fig. 3G), which might have generated inaccurate BIC measurements. In the present study, all implant samples recovered after the push-out test were analyzed by SEM/EDS. The EDS data of Ti weight % was thought to demonstrate the exposed implant surface area (Fig. 3H and J). The EDS element analysis of the exposed Ti weight % showed a clear trend mirroring the BIC with much less variations and thus this measurement was thought to be a viable surrogate measure for BIC. It must be noted that some limitations exist. The purpose of implant therapy is to bear mechanical load, which was not addressed in this model. The limited number of animals may also derive statistical insignificance.

The established mouse implant model was applied to *Npas2* KO mice. We found that the *Npas2 KO* mutation significantly impaired the establishment of osseointegration of SLA implant. *Npas2* ± and *Npas2*−/− mice demonstrated the significant reduction of the implant push-out value (Fig. 5A). Furthermore, while histological bone tissues appeared to be unaffected (Fig. 5B), EDS-based Ti elemental analysis as a surrogate measurement of BIC suggested the decreased bone and implant contact area in the mutant animals (Fig. 5C). Considering that the expression of *Npas2* in BMSC was increased by close contact with Ti substrate, a downstream phenotype of *Npas2* KO mutation may affect the interface tissue (Fig. 5E). The remnant tissue on the recovered implant was likely to be the interface tissue between bone and implant [45,46], and the interface tissue formed in Npas2 ± and Npas2−/− mice lacked the well-organized collagen fibers (Fig. 5F). *Npas2* is a bHLH transcription factor with sequence similarity to a core circadian molecule Clock. However, the lack of its distribution in SCN suggests that *Npas2* may be less involved in the maintenance of core circadian rhythm in the central clock [27,47] but may play more dominant roles in peripheral tissues [48]. Chromatin immunoprecipitation with DNA sequencing (ChIP-Seq) of mouse liver tissue indicated that *Npas2*-associated target genes were not limited to circadian rhythm-related genes [49]. It has been reported that bHLH transcriptional factors affect BMSC differentiation [50–53]. Therefore, we speculate that *Npas2* KO mice did not affect the trabecular bone structure surrounding the implant, but the postulated Ti biomaterial-induced *Npas2*^{hi} interface tissue (Fig. 5G) may be lost resulting in the reduction of osseointegration.

This study further investigated the underlying mechanism of Ti biomaterial-induced *Npas2* using a chemical genetics strategy. Chemical genetics is defined as the study of biological systems using small molecule tools, which may be suited to dissect signal transduction pathways responding to the environmental cues [54,55]. The high throughput screening of pharmacologically active compounds by *Npas2*-LacZ reporter gene expression implicated small molecules with known functions in three pathways. The first group clustered in common functions of modulating intracellular cAMP signaling. The compounds increasing or reducing cAMP were found to reduce or increase *Npas2* expression, respectively (Table 1). The second group was composed of agonists of α2 adrenergic receptors, which increased *Npas2*. The third group was known to disintegrate cytoskeleton, which might decrease BMSC viability resulting in an artificially low detection of *Npas2*-LacZ activity.

Bone homeostasis and regeneration have been intensely investigated through the study of endocrine, paracrine and autocrine mechanisms of bone-related growth factors. The signal transduction of growth factor receptors is mediated, in part, through cAMP and its response elements [56–58]. Adenylate cyclase and cAMP pathway in osteoblasts also mediate the impact of catecholamine receptors such as β-adrenergic receptors. The increased orthotopic bone formation after treatment with "β blockers" in rats [59] and in humans [60,61] was initially postulated to be due to the modulation of cAMP pathway.

Through a series of investigations on Leptin, the hypothalamic-autonomous nervous system (ANS) pathway was found to directly regulate osteoblasts by activating β2-adrenergic receptors [62–64]. Leptin, a hormone derived from adipocytes, activates Leptin-receptor bearing neurons such as proopiomelanocortin/cocaine- and amphetamine-regulated transcript-containing neurons in the hypothalamus [65]. Leptin-influenced hypothalamic activity clearly modulated the vertebral and appendicular bone remodeling through the sympathetic arm of ANS, causing the bone phenotype of Lepin-deficient obese mice [66,67]. The hypothalamic-ANS signal to β2-adrenergic receptor of osteoblasts activates cAMP response element-binding protein (CREB), which transcribes downstream genes including circadian clock, *Per1* and *Per2*. The *Per1/Per2* double knockout mutation reversed the effect of β2-adrenergic receptor agonist and increased the vertebral and appendicular bone architecture [68]. The effect of neurotransmitters on bone remodeling is known as neuroskeletal regulation and is thought to predominantly involve β2-adrenergic receptor of BMSC [62,69].

During the osteogenic differentiation of mouse iPS cells, β2-adrenergic receptor mRNA was found consistently expressed, while α2-adrenergic receptor mRNA was not detected [70]. However, mature os-

teoblasts have been reported to express α-adrenergic receptors [71] albeit much less than β2-adrenergic receptors. The activation of α-adrenergic receptor increased osteoblast proliferation [71,72]. α2-adrenergic receptor knockout mice resulted in contrasting phenotypes between vertebral and appendicular bones [73], suggesting that the hypothalamic-ANS signaling to osteoblasts may be differentially mediated by the repertoire of α- and β-adrenergic receptors and/or osteoblastic circadian clock molecules.

The Chemical Genetics study indicated that α2-adrenergic receptor-related molecular pathways could increase the *Npas2* expression. We postulated that *Npas2* KO mutations might result in the impaired formation of bone-implant interface tissue, resulting in the discrepancy between histological and implant push-out tests. The present study further demonstrated that Ti biomaterials with rough surface robustly upregulated α2-adrenergic receptors of BMSC (Fig. 6E). Thus, we propose that BMSC contacting the SLA implant surface may change its phenotype through increased α2-adrenergic receptors leading to the development of unique *Npas2*^{hi} bone-implant interface tissue, which may play a critical role in osseointegration. α2-adrenergic receptor agonists and β2-adrenergic receptor blockers are commonly used to treat hypertension. A non-selective blocker of β adrenergic receptor was shown to enhance implant osseointegration in rats [74]. Furthermore, a recent retrospective clinical cohort study reported that the use of anti-hypertension medications was associated with a higher dental implant survival [75]. These clinical data are consistent with our hypothesis.

The pathways that underlie osseointegration are undoubtedly complex and multi-factorial. The outcome of this study suggests a novel molecular and cellular pathway contributes to accelerated osseointegration. We propose that alterations in the neuroskeletal regulatory pathway in BMSC is a critical variable determining the establishment of successful osseointegation. The demonstration of Ti biomaterial-induced α2 adrenergic receptor expression and *Npas2* upregulation provides a clear path for the development of therapeutic strategies designed to improve osseointegration or to re-establish implant-bone integration.

Data availability

The raw/processed data required to reproduce these findings cannot be shared at this time due to technical or time limitations. However, they can be provided upon requested.

Acknowledgements

We thank Dr. Manabu Ishijima and Dr. Takahiro Ogwa of the Weintraub Center for Reconstructive Biotechnology, UCLA School of Dentistry for implant surface characterization. We also thank Dr. Robert Damoiseaux, Director of UCLA Molecular Screening Shared Resource for his guidance in high throughput compound screening. Dr. Hirofumi Kido, Department of Oral Rehabilitation, Section of Oral Implantology, Fukuoka Dental College, Fukuoka, Japan and Dr. Yasutomo Yajima, Department of Oral and Maxillofacial Implantology, Tokyo Dental College, Tokyo, Japan are acknowledged for their discussion on data interpretation. This study was supported, in part, by Neobiotech, USA. This investigation was conducted in part in a facility constructed with support from Research Facilities Improvement Program Grant Number C06 RR014529 from the National Center for Research Resources, National Institutes of Health (NCRR/NIH).

Appendix A. Supplementary data

Supplementary data to this article can be found online at https://doi.org/10.1016/j.biomaterials.2018.11.003.

References

[1] F. Guillemot, Recent advances in the design of titanium alloys for orthopedic applications, Expet Rev. Med. Dev. 2 (2005) 741–748.
[2] M. Esposito, H.V. Worthington, P. Thomsen, P. Coulthard, Interventions for replacing missing teeth: different types of dental implants, Cochrane Database Syst. Rev. (2003), CD003815.
[3] P.G. Laing, A.B. Ferguson Jr., E.S. Hodge, Tissue reaction in rabbit muscle exposed to metallic implants, J. Biomed. Mater. Res. 1 (1967) 135–149.
[4] M. Esposito, Y. Ardebili, H.V. Worthington, Interventions for replacing missing teeth: different types of dental implants, Cochrane Database Syst. Rev. (2014), CD003815.
[5] A. Wennerberg, T. Albrektsson, Effects of titanium surface topography on bone integration: a systematic review, Clin. Oral Implants Res. 20 (Suppl 4) (2009) 172–184.
[6] B.D. Boyan, A. Cheng, R. Olivares-Navarrete, Z. Schwartz, Implant surface design regulates mesenchymal stem cell differentiation and maturation, Adv. Dent. Res. 28 (2016) 10–17.
[7] I. Nishimura, Y. Huang, F. Butz, T. Ogawa, A. Lin, C.J. Wang, Discrete deposition of hydroxyapatite nanoparticles on a titanium implant with predisposing substrate microtopography accelerated osseointegration, Nanotechnology 18 (2007).
[8] R.A. Gittens, L. Scheideler, F. Rupp, S.L. Hyzy, J. Geis-Gerstorfer, Z. Schwartz, B.D. Boyan, A review on the wettability of dental implant surfaces II: biological and clinical aspects, Acta Biomater. 10 (2014) 2907–2918.
[9] F. Rupp, R.A. Gittens, L. Scheideler, A. Marmur, B.D. Boyan, Z. Schwartz, J. Geis-Gerstorfer, A review on the wettability of dental implant surfaces I: theoretical and experimental aspects, Acta Biomater. 10 (2014) 2894–2906.
[10] H.W. Meng, E.Y. Chien, H.H. Chien, Dental implant bioactive surface modifications and their effects on osseointegration: a review, Biomark Res. 4 (2016) 24.
[11] J. Kelly, A. Lin, C.J. Wang, S. Park, I. Nishimura, Vitamin D and bone physiology: demonstration of vitamin D deficiency in an implant osseointegration rat model, J. Prosthodont. 18 (2009) 473–478.
[12] G. Dvorak, A. Fugl, G. Watzek, S. Tangl, P. Pokorny, R. Gruber, Impact of dietary vitamin D on osseointegration in the ovariectomized rat, Clin. Oral Implants Res. 23 (2012) 1308–1313.
[13] J. Choukroun, G. Khoury, F. Khoury, P. Russe, T. Testori, Y. Komiyama, G. Sammartino, P. Palacci, M. Tunali, E. Choukroun, Two neglected biologic risk factors in bone grafting and implantology: high low-density lipoprotein cholesterol and low serum vitamin D, J. Oral Implantol. 40 (2014) 110–114.
[14] T. Fretwurst, S. Grunert, J.P. Woelber, K. Nelson, W. Semper-Hogg, Vitamin D deficiency in early implant failure: two case reports, Int. J. Implant. Dent. 2 (2016) 24.
[15] Y. Yamamoto, T. Yoshizawa, T. Fukuda, Y. Shirode-Fukuda, T. Yu, K. Sekine, T. Sato, H. Kawano, K. Aihara, Y. Nakamichi, T. Watanabe, M. Shindo, K. Inoue, E. Inoue, N. Tsuji, M. Hoshino, G. Karsenty, D. Metzger, P. Chambon, S. Kato, Y. Imai, Vitamin D receptor in osteoblasts is a negative regulator of bone mass control, Endocrinology 154 (2013) 1008–1020.
[16] C.M. Mengatto, F. Mussano, Y. Honda, C.S. Colwell, I. Nishimura, Circadian rhythm and cartilage extracellular matrix genes in osseointegration: a genome-wide screening of implant failure by vitamin D deficiency, PloS One 6 (2011), e15848.
[17] W. Liu, S. Zhang, D. Zhao, H. Zou, N. Sun, X. Liang, M. Dard, B. Lanske, Q. Yuan, Vitamin D supplementation enhances the fixation of titanium implants in chronic kidney disease mice, PloS One 9 (2014), e95689.
[18] S.M. Siepka, S.H. Yoo, J. Park, C. Lee, J.S. Takahashi, Genetics and neurobiology of circadian clocks in mammals, Cold Spring Harbor Symp. Quant. Biol. 72 (2007) 251–259.
[19] G. Asher, U. Schibler, A CLOCK-less clock, Trends Cell Biol. 16 (2006) 547–549.
[20] J.D. McElderry, G. Zhao, A. Khmaladze, C.G. Wilson, R.T. Franceschi, M.D. Morris, Tracking circadian rhythms of bone mineral deposition in murine calvarial organ cultures, J. Bone Miner. Res. 28 (2013) 1846–1854.
[21] S. Zvonic, A.A. Ptitsyn, G. Kilroy, X. Wu, S.A. Conrad, L.K. Scott, F. Guilak, G. Pelled, D. Gazit, J.M. Gimble, Circadian oscillation of gene expression in murine calvarial bone, J. Bone Miner. Res. 22 (2007) 357–365.
[22] N. Hassan, K. McCarville, K. Morinaga, C.M. Mengatto, P. Langfelder, A. Hokugo, Y. Tahara, C.S. Colwell, I. Nishimura, Titanium biomaterials with complex surfaces induced aberrant peripheral circadian rhythms in bone marrow mesenchymal stromal cells, PloS One 12 (2017), e0183359.
[23] F. Glon, O. Flys, P.J. Loof, B.G. Rosen, 3D SEM for surface topography quantification - a case study on dental surfaces, J. Phys. Conf. Ser. 483 (2014).
[24] R. Nakao, H. Okauchi, C. Hashimoto, N. Wada, K. Oishi, Determination of reference genes that are independent of feeding rhythms for circadian studies of mouse metabolic tissues, Mol. Genet. Metabol. 121 (2017) 190–197.
[25] R. Yang, Z. Su, Analyzing circadian expression data by harmonic regression based on autoregressive spectral estimation, Bioinformatics 26 (2010) i168–174.
[26] N.M. Bernthal, A.I. Stavrakis, F. Billi, J.S. Cho, T.J. Kremen, S.I. Simon, A.L. Cheung, G.A. Finerman, J.R. Lieberman, J.S. Adams, L.S. Miller, A mouse model of post-arthroplasty Staphylococcus aureus joint infection to evaluate in vivo the efficacy of antimicrobial implant coatings, PloS One 5 (2010), e12580.
[27] J.A. Garcia, D. Zhang, S.J. Estill, C. Michnoff, J. Rutter, M. Reick, K. Scott, R. Diaz-Arrastia, S.L. McKnight, Impaired cued and contextual memory in NPAS2-deficient mice, Science 288 (2000) 2226–2230.
[28] D. Buser, N. Broggini, M. Wieland, R.K. Schenk, A.J. Denzer, D.L. Cochran, B. Hoffmann, A. Lussi, S.G. Steinemann, Enhanced bone apposition to a chemically modified SLA titanium surface, J. Dent. Res. 83 (2004) 529–533.
[29] K.M. Hotchkiss, G.B. Reddy, S.L. Hyzy, Z. Schwartz, B.D. Boyan, R. Olivares-Navarrete, Titanium surface characteristics, including topography and wettability, alter macrophage activation, Acta Biomater. 31 (2016) 425–434.

[30] D.M. Brunette, The effects of implant surface topography on the behavior of cells, Int. J. Oral Maxillofac. Implants 3 (1988) 231–246.
[31] H.C. Lai, L.F. Zhuang, X. Liu, M. Wieland, Z.Y. Zhang, Z.Y. Zhang, The influence of surface energy on early adherent events of osteoblast on titanium substrates, J. Biomed. Mater. Res. 93 (2010) 289–296.
[32] B.A. Warme, N.J. Epstein, M.C. Trindade, K. Miyanishi, T. Ma, R.R. Saket, D. Regula, S.B. Goodman, R.L. Smith, Proinflammatory mediator expression in a novel murine model of titanium-particle-induced intramedullary inflammation, J. Biomed. Mater. Res. B Appl. Biomater. 71 (2004) 360–366.
[33] B. Bragg, N.J. Epstein, T. Ma, S. Goodman, R.L. Smith, Histomorphometric analysis of the intramedullary bone response to titanium particles in wild-type and IL-1R1 knock-out mice: a preliminary study, J. Biomed. Mater. Res. B Appl. Biomater. 84 (2008) 559–570.
[34] R. Jimbo, T. Sawase, Y. Shibata, K. Hirata, Y. Hishikawa, Y. Tanaka, K. Bessho, T. Ikeda, M. Atsuta, Enhanced osseointegration by the chemotactic activity of plasma fibronectin for cellular fibronectin positive cells, Biomaterials 28 (2007) 3469–3477.
[35] L.A. Bonsignore, R.W. Colbrunn, J.M. Tatro, P.J. Messerschmitt, C.J. Hernandez, V.M. Goldberg, M.C. Stewart, E.M. Greenfield, Surface contaminants inhibit osseointegration in a novel murine model, Bone 49 (2011) 923–930.
[36] A. Keuroghlian, A.D. Barroso, G. Kirikian, O. Bezouglaia, Y. Tintut, S. Tetradis, P. Moy, F. Pirih, T. Aghaloo, The effects of hyperlipidemia on implant osseointegration in the mouse femur, J. Oral Implantol. 41 (2015) e7–e11.
[37] D. Chikazu, K. Tomizuka, T. Ogasawara, H. Saijo, T. Koizumi, Y. Mori, Y. Yonehara, T. Susami, T. Takato, Cyclooxygenase-2 activity is essential for the osseointegration of dental implants, Int. J. Oral Maxillofac. Surg. 36 (2007) 441–446.
[38] J.L. Charest, A.J. Garcia, W.P. King, Myoblast alignment and differentiation on cell culture substrates with microscale topography and model chemistries, Biomaterials 28 (2007) 2202–2210.
[39] D.W. Hamilton, D.M. Brunette, The effect of substratum topography on osteoblast adhesion mediated signal transduction and phosphorylation, Biomaterials 28 (2007) 1806–1819.
[40] S. Takeda, F. Elefteriou, R. Levasseur, X. Liu, L. Zhao, K.L. Parker, D. Armstrong, P. Ducy, G. Karsenty, Leptin regulates bone formation via the sympathetic nervous system, Cell 111 (2002) 305–317.
[41] P. Ducy, M. Amling, S. Takeda, M. Priemel, A.F. Schilling, F.T. Beil, J. Shen, C. Vinson, J.M. Rueger, G. Karsenty, Leptin inhibits bone formation through a hypothalamic relay: a central control of bone mass, Cell 100 (2000) 197–207.
[42] T. Albrektsson, P.I. Branemark, H.A. Hansson, J. Lindstrom, Osseointegrated titanium implants. Requirements for ensuring a long-lasting, direct bone-to-implant anchorage in man, Acta Orthop. Scand. 52 (1981) 155–170.
[43] H. Zou, X. Zhao, N. Sun, S. Zhang, T. Sato, H. Yu, Q. Chen, H.P. Weber, M. Dard, Q. Yuan, B. Lanske, Effect of chronic kidney disease on the healing of titanium implants, Bone 56 (2013) 410–415.
[44] Y. Gao, E. Luo, J. Hu, J. Xue, S. Zhu, J. Li, Effect of combined local treatment with zoledronic acid and basic fibroblast growth factor on implant fixation in ovariectomized rats, Bone 44 (2009) 225–232.
[45] J.S. Kim, S.M. Kang, K.W. Seo, K.Y. Nahm, K.R. Chung, S.H. Kim, J.P. Ahn, Nanoscale bonding between human bone and titanium surfaces: osseohybridization, BioMed Res. Int. 2015 (2015) 960410.
[46] L.A. Giannuzzi, D. Phifer, N.J. Giannuzzi, M.J. Capuano, Two-dimensional and 3-dimensional analysis of bone/dental implant interfaces with the use of focused ion beam and electron microscopy, J. Oral Maxillofac. Surg. 65 (2007) 737–747.
[47] M. Reick, J.A. Garcia, C. Dudley, S.L. McKnight, NPAS2: an analog of clock operative in the mammalian forebrain, Science 293 (2001) 506–509.
[48] T. Yamamoto, Y. Nakahata, H. Soma, M. Akashi, T. Mamine, T. Takumi, Transcriptional oscillation of canonical clock genes in mouse peripheral tissues, BMC Mol. Biol. 5 (2004) 18.
[49] N. Koike, S.H. Yoo, H.C. Huang, V. Kumar, C. Lee, T.K. Kim, J.S. Takahashi, Transcriptional architecture and chromatin landscape of the core circadian clock in mammals, Science 338 (2012) 349–354.
[50] H. Miraoui, N. Severe, P. Vaudin, J.C. Pages, P.J. Marie, Molecular silencing of Twist1 enhances osteogenic differentiation of murine mesenchymal stem cells: implication of FGFR2 signaling, J. Cell. Biochem. 110 (2010) 1147–1154.
[51] K.A. Sharff, W.X. Song, X. Luo, N. Tang, J. Luo, J. Chen, Y. Bi, B.C. He, J. Huang, X. Li, W. Jiang, G.H. Zhu, Y. Su, Y. He, J. Shen, Y. Wang, L. Chen, G.W. Zuo, B. Liu, X. Pan, R.R. Reid, H.H. Luu, R.C. Haydon, T.C. He, Hey1 basic helix-loop-helix protein plays an important role in mediating BMP9-induced osteogenic differentiation of mesenchymal progenitor cells, J. Biol. Chem. 284 (2009) 649–659.
[52] T. Iwata, T. Kawamoto, E. Sasabe, K. Miyazaki, K. Fujimoto, M. Noshiro, H. Kurihara, Y. Kato, Effects of overexpression of basic helix-loop-helix transcription factor Dec1 on osteogenic and adipogenic differentiation of mesenchymal stem cells, Eur. J. Cell Biol. 85 (2006) 423–431.
[53] S. Yi, M. Yu, S. Yang, R.J. Miron, Y. Zhang, Tcf12, a member of basic helix-loop-helix transcription factors, mediates bone marrow mesenchymal stem cell osteogenic differentiation in vitro and in vivo, Stem Cell. 35 (2017) 386–397.
[54] S.M. Carlson, F.M. White, Using small molecules and chemical genetics to interrogate signaling networks, ACS Chem. Biol. 6 (2011) 75–85.
[55] F. Cong, A.K. Cheung, S.M. Huang, Chemical genetics-based target identification in drug discovery, Annu. Rev. Pharmacol. Toxicol. 52 (2012) 57–78.
[56] M. Mezawa, S. Araki, H. Takai, Y. Sasaki, S. Wang, X. Li, D.S. Kim, Y. Nakayama, Y. Ogata, Regulation of human bone sialoprotein gene transcription by platelet-derived growth factor-BB, Gene 435 (2009) 80–87.
[57] S.F. Liou, J.H. Hsu, H.C. Chu, H.H. Lin, I.J. Chen, J.L. Yeh, KMUP-1 promotes osteoblast differentiation through cAMP and cGMP pathways and signaling of BMP-2/smad1/5/8 and wnt/beta-catenin, J. Cell. Physiol. 230 (2015) 2038–2048.
[58] W. Zhou, L. Yu, J. Fan, B. Wan, T. Jiang, J. Yin, Y. Huang, Q. Li, G. Yin, Z. Hu, Endogenous parathyroid hormone promotes fracture healing by increasing expression of BMPR2 through cAMP/PKA/CREB pathway in mice, Cell. Physiol. Biochem. 42 (2017) 551–563.
[59] B. Minkowitz, A.L. Boskey, J.M. Lane, H.S. Pearlman, V.J. Vigorita, Effects of propranolol on bone metabolism in the rat, J. Orthop. Res. 9 (1991) 869–875.
[60] S. Turker, V. Karatosun, I. Gunal, Beta-blockers increase bone mineral density, Clin. Orthop. Relat. Res. 443 (2006) 73–74.
[61] J.A. Pasco, M.J. Henry, K.M. Sanders, M.A. Kotowicz, E. Seeman, G.C. Nicholson, S. Geelong Osteoporosis, Beta-adrenergic blockers reduce the risk of fracture partly by increasing bone mineral density: geelong Osteoporosis Study, J. Bone Miner. Res. 19 (2004) 19–24.
[62] M.S. Patel, F. Elefteriou, The new field of neuroskeletal biology, Calcif. Tissue Int. 80 (2007) 337–347.
[63] C.J. Rosen, Bone remodeling, energy metabolism, and the molecular clock, Cell Metabol. 7 (2008) 7–10.
[64] G. Karsenty, Convergence between bone and energy homeostases: leptin regulation of bone mass, Cell Metabol. 4 (2006) 341–348.
[65] B. Meister, Control of food intake via leptin receptors in the hypothalamus, Vitam. Horm. 59 (2000) 265–304.
[66] J.C. Fleet, Leptin and bone: does the brain control bone biology?, Nutr. Rev. 58 (2000) 209–211.
[67] G. Karsenty, Leptin controls bone formation through a hypothalamic relay, Recent Prog. Horm. Res. 56 (2001) 401–415.
[68] L. Fu, M.S. Patel, A. Bradley, E.F. Wagner, G. Karsenty, The molecular clock mediates leptin-regulated bone formation, Cell 122 (2005) 803–815.
[69] G.J. Spencer, I.S. Hitchcock, P.G. Genever, Emerging neuroskeletal signalling pathways: a review, FEBS Lett. 559 (2004) 6–12.
[70] S. Nagao, T. Goto, S. Kataoka, T. Toyono, T. Joujima, H. Egusa, H. Yatani, S. Kobayashi, K. Maki, Expression of neuropeptide receptor mRNA during osteoblastic differentiation of mouse iPS cells, Neuropeptides 48 (2014) 399–406.
[71] H.H. Huang, T.C. Brennan, M.M. Muir, R.S. Mason, Functional alpha1- and beta2-adrenergic receptors in human osteoblasts, J. Cell. Physiol. 220 (2009) 267–275.
[72] D. Kodama, A. Togari, Noradrenaline stimulates cell proliferation by suppressing potassium channels via G(i/o) -protein-coupled alpha(1B) -adrenoceptors in human osteoblasts, Br. J. Pharmacol. 168 (2013) 1230–1239.
[73] M.B. Cruz Grecco Teixeira, G.M. Martins, M. Miranda-Rodrigues, I.F. De Araujo, R. Oliveira, P.C. Brum, C.H. Azevedo Gouveia, Lack of alpha2C-Adrenoceptor Results in Contrasting Phenotypes of Long Bones and Vertebra and Prevents the Thyrotoxicosis-Induced Osteopenia, PloS One 11 (2016), e0146795.
[74] A.E. Al-Subaie, M. Laurenti, M.N. Abdallah, I. Tamimi, F. Yaghoubi, H. Eimar, N. Makhoul, F. Tamimi, Propranolol enhances bone healing and implant osseointegration in rats tibiae, J. Clin. Periodontol. 43 (2016) 1160–1170.
[75] X. Wu, K. Al-Abedalla, H. Eimar, S. Arekunnath Madathil, S. Abi-Nader, N.G. Daniel, B. Nicolau, F. Tamimi, Antihypertensive medications and the survival rate of osseointegrated dental implants: a cohort study, Clin. Implant Dent. Relat. Res. 18 (2016) 1171–1182.